NAVAL POSTGRADUATE SCHOOL
MONTEREY, CALIFORNIA



THESIS

OBSERVATIONS AND CHARACTERIZATIONS OF NON-LINEAR INTERNAL WAVES ON THE MID-ATLANTIC BIGHT CONTINENTAL SHELF

by

Donald W. Taube

June, 1996

Thesis Advisor: Ching-Sang Chiu
Second Reader: Thomas H.C. Herbers

Approved for public release; distribution is unlimited.

DUDLEY KNOX LIBRARY
NAVAL POSTGRADUATE SCHOOL
MONTEREY CA 93943-5101

REPORT DOCUMENTATION PAGE

Form Approved OMB No. 0704-0188

Public reporting burden for this collection of information is estimated to average 1 hour per response, including the time for reviewing instruction, searching existing data sources, gathering and maintaining the data needed, and completing and reviewing the collection of information. Send comments regarding this burden estimate or any other aspect of this collection of information, including suggestions for reducing this burden, to Washington Headquarters Services, Directorate for Information Operations and Reports, 1215 Jefferson Davis Highway, Suite 1204, Arlington, VA 22202-4302, and to the Office of Management and Budget, Paperwork Reduction Project (0704-0188) Washington DC 20503.

1. AGENCY USE ONLY *(Leave blank)*	2. REPORT DATE June 1996.	3. REPORT TYPE AND DATES COVERED Master's Thesis

4. TITLE AND SUBTITLE OBSERVATIONS AND CHARACTERIZATIONS OF NON-LINEAR INTERNAL WAVES ON THE MID-ATLANTIC BIGHT CONTINENTAL SHELF

5. FUNDING NUMBERS

6. AUTHOR(S) Donald W. Taube

7. PERFORMING ORGANIZATION NAME(S) AND ADDRESS(ES)
Naval Postgraduate School
Monterey CA 93943-5000

8. PERFORMING ORGANIZATION REPORT NUMBER

9. SPONSORING/MONITORING AGENCY NAME(S) AND ADDRESS(ES)
Office of Naval Research

10. SPONSORING/MONITORING AGENCY REPORT NUMBER

11. SUPPLEMENTARY NOTES The views expressed in this thesis are those of the author and do not reflect the official policy or position of the Department of Defense or the U.S. Government.

12a. DISTRIBUTION/AVAILABILITY STATEMENT
Approved for public release; distribution is unlimited.

12b. DISTRIBUTION CODE

13. ABSTRACT *(maximum 200 words)*

During the summer of 1995, an intensive, joint field study called Shallow Water Acoustics in a Random Medium (SWARM '95) was conducted by the Naval Research Laboratories (NRL), Woods Hole Oceanographic Institution (WHOI), University of Delaware (UD), Applied Physics Laboratory of Johns Hopkins University (APL/JHU) and Naval Postgraduate School (NPS), among others, in the Mid-Atlantic Bight continental shelf region off the coast of New Jersey. Environmental and acoustic sensors were deployed as part of SWARM '95 to measure and characterize the non-linear internal waves and their impact on the spatial and temporal coherence of the acoustic transmissions. As part of the environmental monitoring network, two bottom-moored, upward looking Acoustic Doppler Current Profilers (ADCPs) were deployed. A modal, time-series analysis of the data captured by the two ADCPs was performed. Highlights of the results reveal that: the generation mechanism, in this case, is consistent with the lee-wave hypothesis of generation; the phase speed is in good agreement with predicted phase speeds of the first baroclinic mode; and, the displacement power spectral density is significantly modified when soliton wavepackets are present.

14. SUBJECT TERMS Solitons, ADCP, Internal Waves, Mid-Atlantic Bight, Continental Shelf			15. NUMBER OF PAGES 63 16. PRICE CODE
17. SECURITY CLASSIFICATION OF REPORT Unclassified	18. SECURITY CLASSIFICATION OF THIS PAGE Unclassified	19. SECURITY CLASSIFICATION OF ABSTRACT Unclassified	20. LIMITATION OF ABSTRACT UL

NSN 7540-01-280-5500

Standard Form 298 (Rev. 2-89)
Prescribed by ANSI Std. 239-18 298-102

Approved for public release; distribution is unlimited.

OBSERVATIONS AND CHARACTERIZATIONS OF NON-LINEAR INTERNAL WAVES ON THE MID-ATLANTIC BIGHT CONTINENTAL SHELF

Donald W. Taube
Lieutenant Commander, United States Navy
B.A., University of California at Santa Barbara, 1977
M.A., University of California at Santa Barbara, 1981

Submitted in partial fulfillment
of the requirements for the degree of

MASTER OF SCIENCE IN METEOROLOGY AND PHYSICAL OCEANOGRAPHY

from the

NAVAL POSTGRADUATE SCHOOL
June 1996

DUDLEY KNOX LIBRARY
NAVAL POSTGRADUATE SCHOOL
MONTEREY CA 93943-5101

ABSTRACT

During the summer of 1995, an intensive, joint field study called Shallow Water Acoustics in a Random Medium (SWARM '95) was conducted by the Naval Research Laboratories (NRL), Woods Hole Oceanographic Institution (WHOI), University of Delaware (UD), Applied Physics Laboratory of Johns Hopkins University (APL/JHU) and Naval Postgraduate School (NPS), among others, in the Mid-Atlantic Bight continental shelf region off the coast of New Jersey. Environmental and acoustic sensors were deployed as part of SWARM '95 to measure and characterize the non-linear internal waves and their impact on the spatial and temporal coherence of the acoustic transmissions. As part of the environmental monitoring network, two bottom-moored, upward looking Acoustic Doppler Current Profilers (ADCPs) were deployed. A modal, time-series analysis of the data captured by the two ADCPs was performed. Highlights of the results reveal that: the generation mechanism, in this case, is consistent with the lee-wave hypothesis of generation; the phase speed is in good agreement with predicted phase speeds of the first baroclinic mode; and, the displacement power spectral density is significantly modified when soliton wavepackets are present.

TABLE OF CONTENTS

I. INTRODUCTION 1

A. MOTIVATION AND THESIS OBJECTIVES 1

B. SWARM '95 3

C. A REVIEW OF SOLITON OBSERVATIONS 6

II. DATA AND PROCESSING METHODS 13

A. ADCP MEASUREMENT GEOMETRY 13

B. DATA PROCESSING 14
1. Re-orientation 14
2. Vertical EOF decomposition 15
3. Temporal Filtering 18

III. ANALYSIS 23

A. GENERATION 23

B. DYNAMICAL MODAL RELATIONS 26

C. SOLITON PROPAGATION 32

D. DISPLACEMENT POWER SPECTRAL DENSITY 39

VI. CONCLUSIONS 45

LIST OF REFERENCES 47

INITIAL DISTRIBUTION LIST 49

LIST OF SYMBOLS

Chapter 2

D	distance between successve soliton wave packets (km)
h_1	depth of mixed layer (m)
h_2	depth of lower layer (m)
l_s	width of surface expression of soliton wave (m)
L	Length of soliton wavepacket (m)
R_c	propagation distance of a soliton wave packet (km)
W	along-slope distance of soliton (km)
η_0	displacement of initial wave of soliton wavepacket (m)
λ_0	distance between surface expression of successive soliton waves (m)
ρ	density (of either mixed player or lower layer)

Chapter 3

D	data matrix
D^T	transpose of data matrix
DD^T	covariance matrix
e_i	column eigenvectors of data matrix - the vertical EOFs
m_i	modal amplitude time-series created by projecting the data onto the mode
u	along-slope particle velocity
v	upslope particle velocity
w	vertical particle velocity
λ_i^2	eigenvalues from the covariance matrix - relative distribution of kinetic energy in each of the EOFs

Chapter 5

c_n	linear soliton phase speed
C_n	non-linear soliton phase speed
f	frequency
F_n	vertical modes of horizontal motion
H	water depth
q_n	normalization constant for Fn
$^{(s)}$	modal amplitudes associated with solitons
s_n/k_n	parameters describing degree of non-linearity in relations between ηn and v'n and ηn and wn
t	time
u_n	modal coefficients describing the along-slope temporal structure
v_n	modal coefficients describing the upslope temporal structure
v'_n	particle velocity parallel to y'
w_n	modal coefficients describing the vertical temporal structure
W_n	vertical modes of vertical displacement
y'	direction of propagation of wavefront
z	depth
α_n/β_n	environmental parameters accounting for effects of buoyancy, current, current shear and water depth
Δ_n	soliton non-linear characteristic width
η_n	modal coefficients describine the displacement temporal structure
$\eta_{0,n}$	peak modal smplitude of soliton

ACKNOWLEDGEMENTS

This project could not have been completed without funding for the Shalow Water Acoustics in a Random Medium (SWARM 95) by the Office of Naval Research.

Some people liken the task of writing a thesis to that of giving birth to a baby; the long gestation period, the final intense labor, and the pride in having brought something new into the world. In keeping with that analogy, I am completely fortunate that this thesis was taken by Caeserian section by my advisor, Dr. Ching-Sang Chiu. He rolled up his sleeves, reached in up to his elbows and lifted this thesis out of me an in act for which I am forever greatful. I am also most grateful to Dr. Thomas Herbers for allowing me to bring him onboard long past the time that would have been considered late, and providing the help, encouragement and comments that made the thesis complete.

My lab-mate, and near-Siamese twin, LCDR Anthony D'Agostino, was my inspiration as he moved briskly to get his research done in an orderly manner. Chris Miller and Stefan Hudson were saintly in their patience with my repeatedly ill-informed questions. Were it not for Todd Anderson and Rich Schramm of Monterey Bay Aquarium Research Institute (MBARI), I would still be trying to get incomprehensible data into a processable form, so thank you.

Ms. Marla Stone helped start this project and will, hopefully, be able to sift through the ashes to carry the findings forward. Mr. Steven Taylor and Mr. Bob Creasy were gracious enough to provide meteorological data to support one hypothesis. Thanks to those nice people at the MATH WORKS for making MATLAB; the only language I could have used to conduct this analysis.

Most crucially, I am in the deepest debt to my wife, Chris, and my children, Sara and Billyum, for indulging me with their patience despite my repeated absences during the excruciatingly long time this endeavor required.

I. INTRODUCTION

A. MOTIVATION AND THESIS OBJECTIVES

In conducting naval operations near any coast, an intimate knowledge of the barotropic tide has long been regarded as a minimum requirement to enhance safety. Through centuries of study, barotropic tides have become sufficiently well understood to allow accurate prediction of sea-level heights and tidal currents within littoral regions. Unfortunately, the ability to predict tidal motions throughout the water column above the continental slope and shelf is not as well understood. When the barotropic tide interacts with complex bathymetry, enhanced meteorological forcing and the often-stratified vertical density structure of the water mass above the shelf, it can couple energy into baroclinic modes. As a result of this coupling, internal waves, both linear and non-linear, abound in the water above the continental shelf. Of particular interest are non-linear internal waves, some of which have been described as solitary waves (solitons). Although they are internal waves and their predominant impact is as disturbances within the water column, solitons may exhibit a surface manifestation of intermittent choppy and glassy seas. In the water column, the internal disturbances caused by non-linear internal waves have been observed to be significant enough to potentially impact naval operations

above the continental shelf. Consequently, as naval operations continue to move into littoral regions, gaining a better understanding of non-linear internal waves may be as important to safe naval operations as has been determining the phase of the barotropic tide.

The focus of this thesis is on a physical description of the non-linear internal wave packets, formed near the shelfbreak and traveling shoreward on the Mid-Atlantic Bight continental shelf. Specifically, Acoustic Doppler Current Profiler (ADCP) measurements, obtained from two moorings above the continental shelf, are analyzed in an effort to answer the following questions:

1. What is the generation mechanism?
2. What are the propagation characteristics?
3. What are the spectral characteristics?

The ADCP measurements were conducted as part of the 1995 Shallow Water Acoustics in a Random Medium experiment (SWARM '95). The SWARM '95 experimental region is shown in Figure 1, along with the bathymetry and locations of the two ADCPs.

The organization of this thesis is as follows: A background on SWARM '95 and a brief review of previous observations of non-linear internal waves are presented in the remainder of this Chapter. The geometry of the ADCP measurements and the data processing method used in this study are discussed in Chapter II. Analyses on the

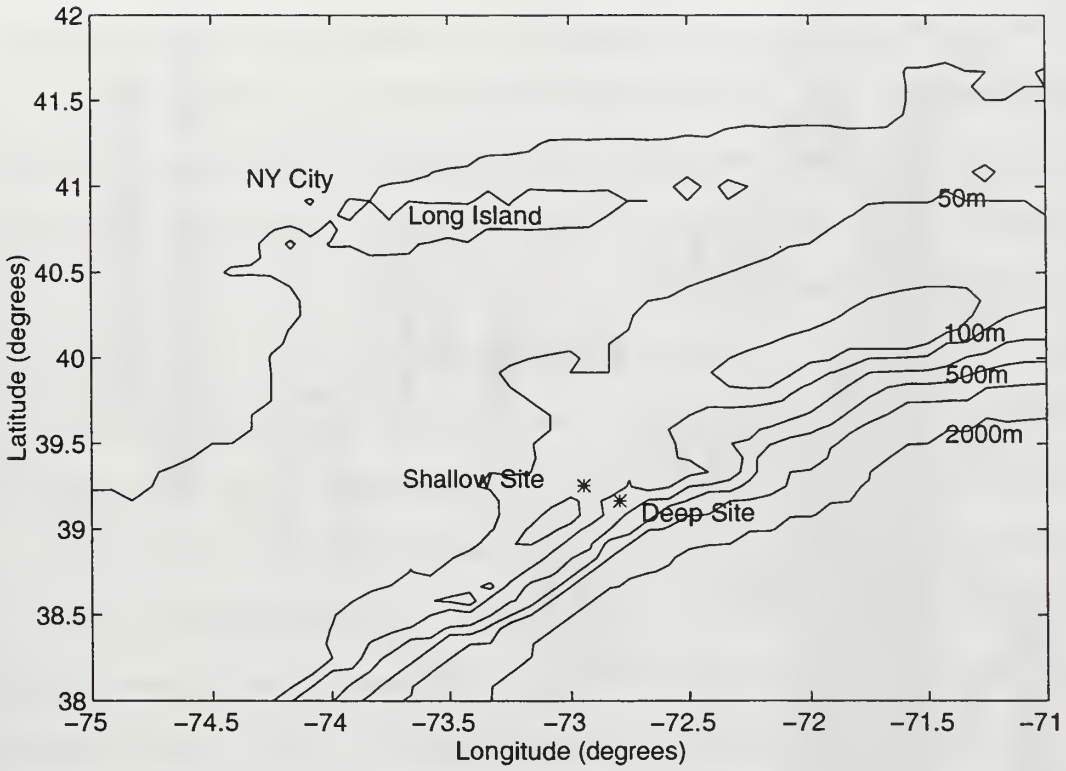


Figure 1. Locations of the ADCPs in SWARM '95.

generation mechanism, propagation characteristics and spectral characteristics are presented in Chapter III. Conclusions are summarized in Chapter IV.

B. SWARM '95

Under the sponsorship of the Office Of Naval Research (ONR), SWARM '95 took place during 20 July to 12 August 1995 in the Mid-Atlantic Bight continental shelf region off the coast of New Jersey (see Figure 1). The primary objective of this experiment was to quantify the interaction of 10-2000 Hz acoustic signals with shallow water linear and non-linear internal waves. In order to accomplish this

objective, very high quality physical oceanographic data and bottom geoacoustic data were collected along with acoustic transmission data. In addition to supporting the acoustic measurements, the oceanographic data were of sufficient quality to support studies of generation, propagation and dissipation of the internal waves within the shelf region.

SWARM '95 was a large, multi-institution, multi-investigator project. Investigators from the Naval Research Laboratories (NRL), Woods Hole Oceanographic Institution (WHOI), University of Delaware, and the Applied Physics Laboratory of Johns Hopkins University (APL/JHU) participated directly in the cruise. Investigators from Naval Postgraduate School (NPS), University of Rhode Island (URI), Scripps Institute of Oceanography (SIO), University of Miami, and Northeastern University contributed equipment and/or participated in the analysis. NPS contributed two Acoustic Doppler Current Profilers (ADCPs) and subsequently analyzed the measured time-series.

The collection of the acoustic and oceanographic data during SWARM '95 involved three research vessels working at the experimental site, two of which occupied the site for the full duration of SWARM. The collection included successful deployment and recovery of twenty-five oceanographic and/or acoustic moorings. A representation of the environmental data collection effort is provided in Figure 2. The environmental measurements included those

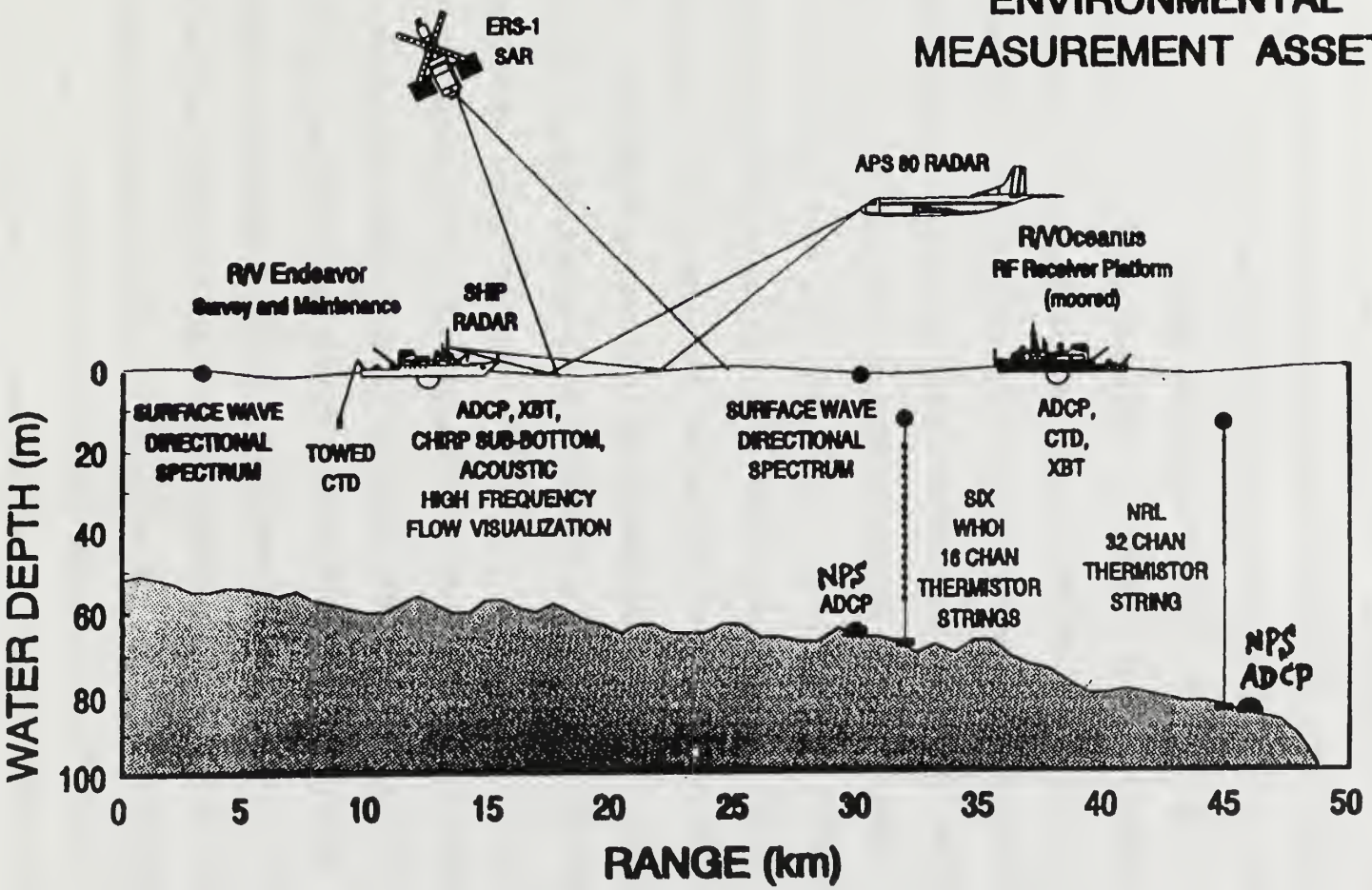


Figure 2. A schematic of the environmental measurement assets involved with data collection during SWARM '95 (Courtesy of NRL and WHOI).

from: two bottom-moored ADCPs, thermistor chains, expendable bathythermographs (XBTs), a towed conductivity temperature depth (CTD) sensor, CTD casts, a vessel-mounted ADCP along with imagery from spaceborne and airborne Synthetic Aperture Radar (SAR) systems and shipborne radar imagery.

C. A REVIEW OF SOLITON OBSERVATIONS

The name of "SWARM" includes the words "random medium." This refers to the environmental fluctuations caused by internal waves, particularly the non-linear internal wave packets, present in the continental shelf. These waves have been described as solitary waves, or solitons, and will be discussed herein.

Scientific literature is rich in articles describing solitons in numerous contexts, including: nuclear physics, electron-positron plasmas, optical waveguides and communications, charged particle energization, conducting polymers and others, including oceanography. Of particular interest to this thesis are solitons in shallow water.

According to Osborne and Burch (1980), surface solitons were first observed by John Scott Russell in the 19th century and Korteweg-de Vries (KdV) published a theoretical article about solitons in 1895. Theoretical papers about internal solitons were written in the 1950s and 1960s, including those by Long (1953, 1956) and Davis and Acrivos (1967). Thereafter, numerous empirical results and theoretical considerations have been published.

Some relevant features regarding internal solitons are:

1) These waves are usually observed in summer when they are trapped in a strong and shallow seasonal thermocline. [Farmer and Smith (1980); Loder *et al.* (1992)]

2) The solitary waveforms are depressions in the pycnocline and often have a "$sech^2$" profile. [Chereskin (1983)] When an initial solitary wave propagates, it often evolves more rank-ordered solitons and exhibits clear non-linear and dispersive features such as higher-than-linear group velocity, and a decrease in wavelength and amplitude toward the rear of the packet. [Farmer and Smith (1980)]

3) Solitary waves propagate shoreward, and are often generated by a tidally driven flow over sills, continental shelf edges, or other major variation in the underwater topography. [Chereskin (1983), Loder *et al.* (1992)] Internal waves have also been observed propagating seaward, but will not be discussed here.

4) Because of the shallowness of the summer seasonal thermocline and the large amplitude of the coastal internal waves, strong surface expressions of solitons have been observed with a variety of remote sensors, including photographs and synthetic aperture radar (SAR) from satellites and space shuttles. [Apel (1978, 1995), Chereskin (1983)]

Figure 3 provides a schematic plan view and profile of a soliton packet, with typical scales listed in Table 1. A

spaceborne synthetic aperture radar (SAR) image of the surface expression of actual solitons in the vicinity of the Mid-Atlantic Bight continental shelf is presented in Figure 4. The solitons are the quasi-linear features throughout Figure 4, most strikingly is the band from the bottom center to the upper-right corner of the image.

Naturally occurring, large-amplitude internal solitons have been reported in many coastal zones of the world such as: the Massachusetts Bay, the New York Bight, Gulf of California, Andaman Sea offshore of Thailand, the Australian North West Shelf, the Sulu Sea between the Philippines and Borneo, off the coast of Portugal, off Hainan Island in the South China Sea, off the Strait of Gibraltar in the Alboran Sea, the Scotian Shelf off Nova Scotia, the Celtic Sea and so on. They have also been observed in lakes. [Zhou *et al.* (1991)] Apel *et al.* (1975) have also located surface manifestations of solitons off southwest Africa and off equatorial east Africa in the Indian Ocean, while Munro (1982) reports on solitons in the Davis Strait.

Internal solitons can have significant amplitudes. Loder *et al.* (1992) noted that during towed Conductivity Temperature Depth (CTD) observations above the Northern Georges Banks, solitons with vertical amplitudes of 10-40 meters and horizontal scales ranging from several hundred meters to several kilometers were found. Loder *et al.* (1992) went on to note that these observations were

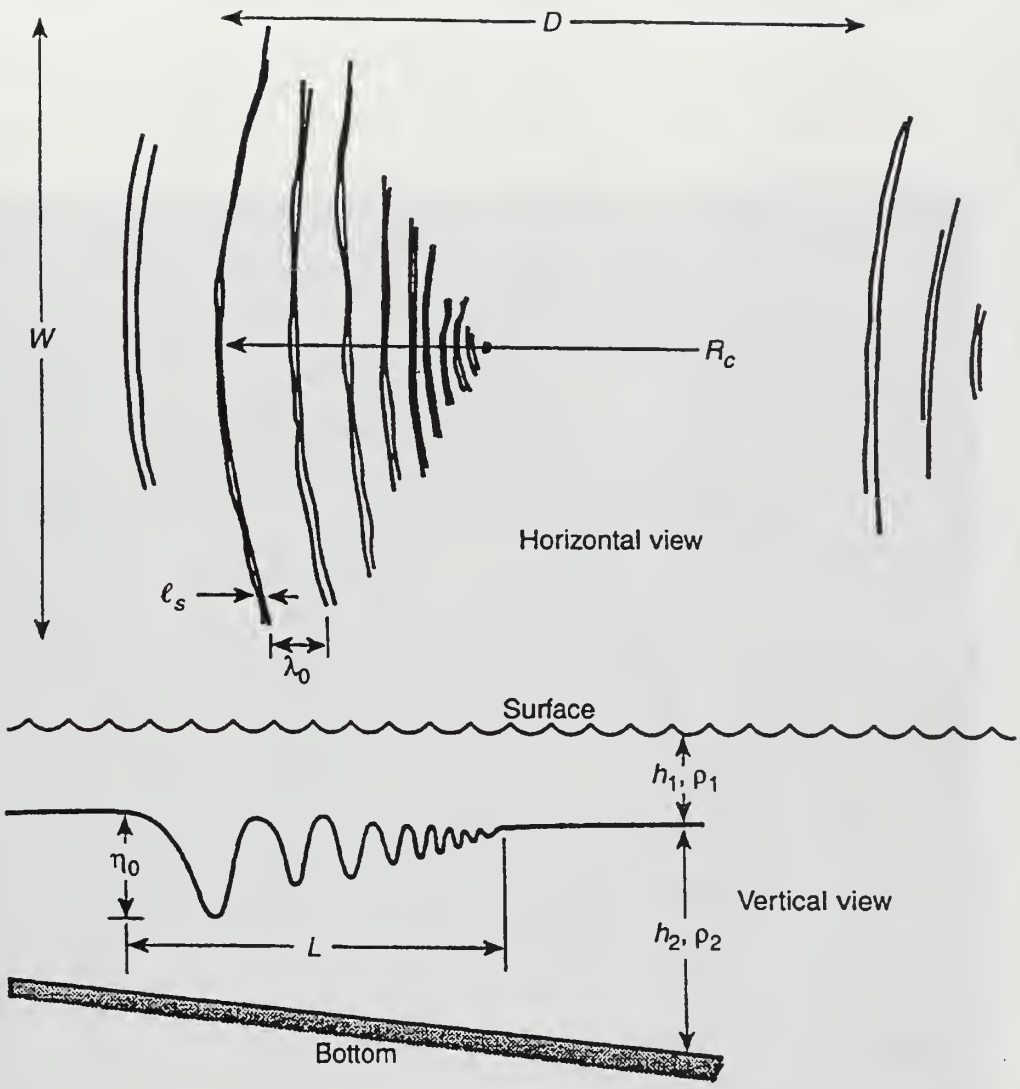


Figure 3 Schematic plan view and profile of soliton waves (from Apel 1995).

Table 1. Typical Scales for Continental Shelf Solitons (after Apel, 1995)

L (km)	η_0 (m)	h_1 (m)	h_2 (m)	l_s (m)
1-5	0-15	20-25	100	100
λ_0 (m)	W (km)	D (km)	Rc (km)	$\Delta\rho/\rho$
50-500	0-30	15-25	25-4	0.001

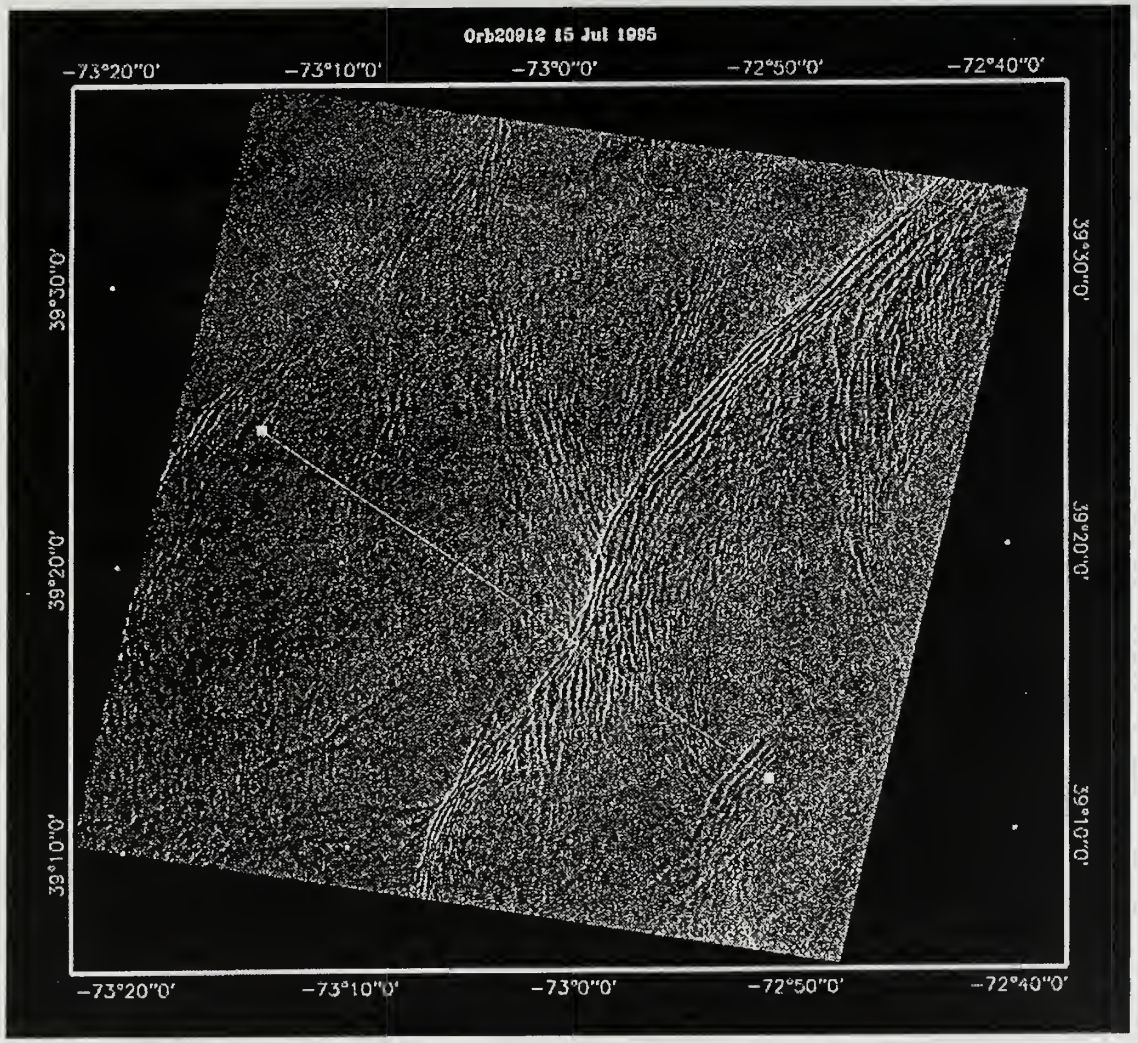


Figure 4. ERS-1 synthetic aperture radar (SAR) image of the surface expression of actual solitons in the vicinity of the Mid-Atlantic Bight continental shelf (from Apel, 1995). The solitons are the bright quasi-linear features throughout the image, although the band from the bottom center to the upper-right corner is most prominent. The white line connecting the white dots represents the SWARM experimental site.

consistent with numerous observations by other researchers, including: Farmer and Smith (1980); Chereskin (1983); Sandstrom and Elliot (1984); Holloway (1987), as well as others. Holloway (1987) describes a bore (soliton) that propagates shoreward which produces up to 60 m drops in the isotherms, although the 30 minute sampling interval he employed may not accurately depict the velocities and structure of these solitons.

No direct effect on naval operations has been documented, although these waves have been cited as potentially overwhelming the station-keeping capabilities of the dynamic positioning systems of offshore drilling ships [Osborne *et al.* (1978), Munro (1982)]. Consequently, solitons may also impact naval operations in the following ways:

1. disruption of moored mine fields,

2. uncontrolled motions of both enemy mines and friendly mine clearing equipment during Mine-Counter-Measures operations,

3. sudden "depth excursions" by special warfare divers while approaching/leaving coastal waters while submerged,

4. sudden "depth excursions" by submerged submarines while operating above or near the continental shelf,

5. disruption of acoustic paths while localizing and/or prosecuting enemy submarines in shallow water.

Considering their pervasiveness, significant amplitude

and possibly significant tactical effect, some explanation of the generation and propagation of these waves is in order.

II. DATA AND PROCESSING METHODS

A. ADCP MEASUREMENT GEOMETRY

As part of the SWARM environmental monitoring network, two RD Instruments (RDI) Self-Contained Acoustic Doppler Current Profilers (SC-ADCPs) were moored 4 m above the seafloor, facing upward, at two separate locations, 16.5 km apart, along the experimental track. While one of them was placed in 103 m of water at 39° 10.000'N, 72° 47.416'W near the shelf-break (hereafter referred to as the "Deep Site"), the other one was in 75 m of water at 39° 25.33369'N, 72° 56.5942'W ("Shallow Site" hereafter). Each ADCP was configured to transmit 225 pings per ensemble, with an ensemble sampling interval of 90 seconds. The acoustic frequency for the pings was 307.2 kHz. The four upward projected beams were oriented thirty degrees from the vertical and the data were recorded in earth coordinates (north, east and up each being positive). Each ADCP had a 4 m sampling blank directly above the transmitter head, then it sensed the water column in 4 m long depth bins. With these settings of profiling parameters, the current velocity measurements were accurate to approximately 1 cm/s.

Measurements at the Shallow Site were collected in 16 depth bins centered from 67 m to 7 m below the surface. At the Deep Site, the data was obtained in 22 depth bins centered from 95 m to 11 m below the sea surface. Thus, the

resultant ADCP data set comprises time series of depth profiles of three-dimensional current velocities with a sampling time interval of 90 s and a depth interval of 4 m. While the Deep-Site time series encompasses data from Julian date (JD) 204 to JD 221, the Shallow-Site time series is 4 days shorter, containing data between JD 209 and JD 222.

B. DATA PROCESSING

The processing of the ADCP data entailed three successive steps. The first step was axis re-orientation followed by vertical empirical-orthogonal-mode (EOF) decompositions. The final step involved temporal filtering of the modal coefficients/amplitudes. The filtering enabled the decomposition of the ocean variability of three different time scales; synoptic, tidal and buoyancy. The understanding of soliton production and propagation may be gained by studying the relationships between meteorological events, the barotropic and internal tides and buoyancy motion. The three successive data processing steps, along with some important results, are discussed in the following.

1. Re-orientation

For the ease of the oceanographic analysis, a regular coordinate system (x,y,z) with the y axis pointing shoreward (i.e., upslope) and matching the line that joins the two ADCPs was introduced. With respect to the earth-oriented coordinates, the y-direction is 306° True. The x-axis has an along-slope orientation pointing to 36° True. The z-axis

is positive upward with z=0 being the sea surface. The direction re-orientation was completed by projecting the measured currents, which were in earth-oriented coordinates, onto this (x,y,z) coordinate system. The current vector in (x,y,z) is denoted hereafter by (u,v,w).

2. Vertical EOF Decomposition

The time-series of the three particle velocity components, upslope (v), along-slope (u) and vertical (w), profiled at the Deep and Shallow Sites, were then subjected to vertical EOF decompositions. For each velocity component at each site, the data covariance matrix was formed and its eigenvalues and eigenvectors computed. Mathematically, the decomposition can be cast as a linear-algebra problem:

$$(DD^T)e_i = \lambda_i^2 e_i \qquad (1)$$

where D is the data matrix with each row containing the time samples at each depth bin and thus the columns correspond to depth profiles, and DD^T is the data covariance matrix with D^T denoting the matrix transpose of D. The column eigenvectors (e_i) of DD^T are the vertical EOFs and the eigenvalues (λ_i^2) denote the relative distribution of the kinetic energy in each of the empirical modes of the velocity component being processed. After the EOFs are computed, the time series of the corresponding modal amplitude, m_i, can be easily obtained by projecting the data onto the mode:

$$m_i = d_i^T D \quad . \tag{2}$$

Alternatively, one may choose to project the data onto the dynamical (i.e., theoretical) modes. However, it is rather appealing to calculate vertical modes independently of theory, so that the purely empirical results can be used to validate the theory. In the bottom half of Figure 5, all the "significant" Shallow-Site EOF modes are displayed, except for the zeroth (i.e., barotropic) mode of horizontal current which is approximately uniform. By "significant", it is meant that these modes have root-mean-square velocities twice as large as the ADCP measurement error of 1 cm/s. The bottom left panel shows the 1st and 2nd baroclinic EOFs of the horizontal current while the bottom right panel shows the only significant EOF for displacement (w). It is important to point out that the EOFs for u and v are almost identical. Modes observed at the Deep Site are similar to those of the Shallow Site. The eigenvalues also indicate that the first three EOFs for u and v encompassed over 93% of the total horizontal kinetic energy at both the Shallow and Deep Sites.

For comparison, the predicted vertical structure based on theory is displayed on the top half of Figure 5. These dynamical modes were calculated using a buoyancy frequency profile (see Figure 6) derived from a CTD cast at a location between the two ADCPs. The EOFs and dynamical modes for the

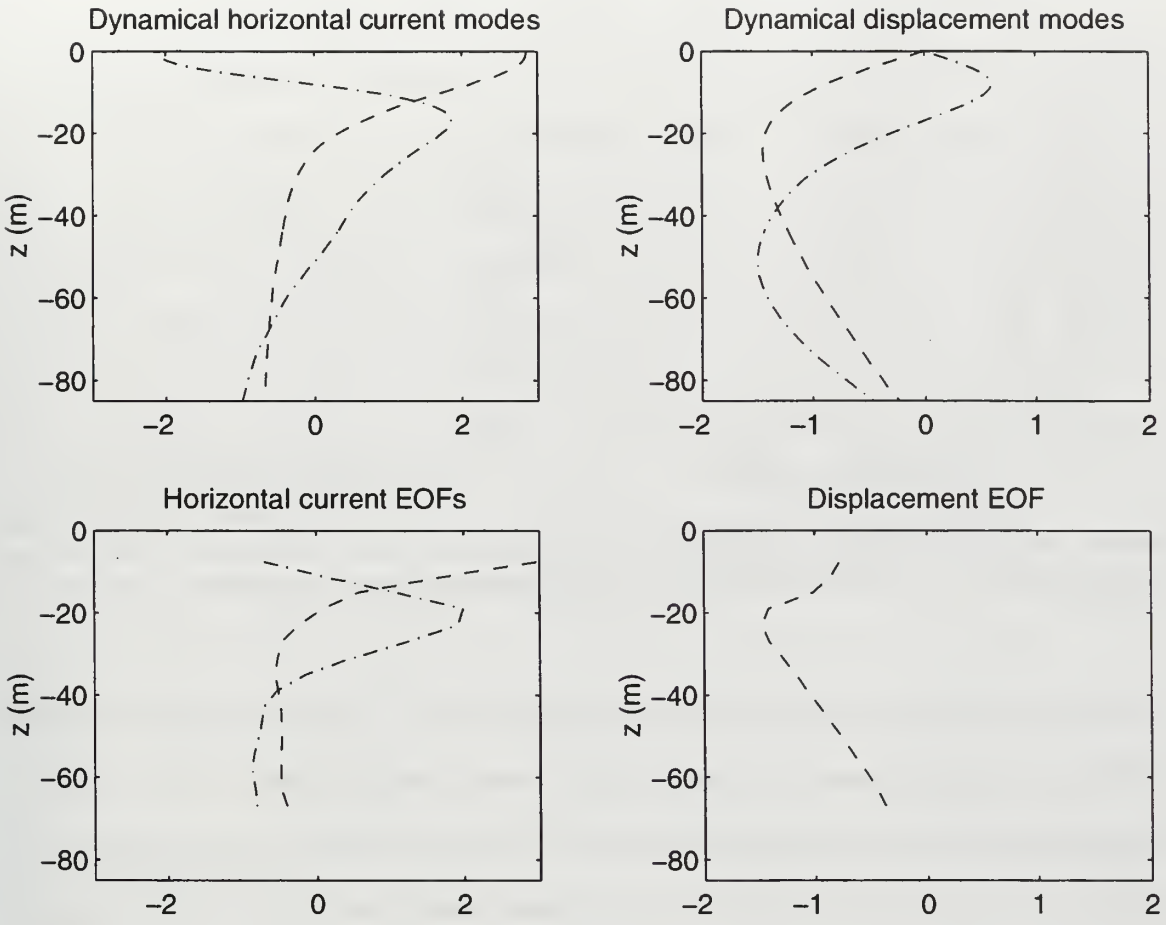


Figure 5. Vertical structure of currents (left panels) and displacements (right panels). Dynamical modes calculated based on an observed buoyancy profile are shown on the top panels whereas the vertical empirical orthogonal functions derived from the ADCP data are shown on the bottom panels for comparison. First baroclinic mode is denoted by dashed lines and second mode by dot-dashed lines. The zeroth barotropic mode is not shown.

horizontal currents are strikingly similar. However, as for the vertical current, dissimilarities between the EOF and the 1st baroclinic dynamical mode can be easily observed. An explanation is that the EOF for w may actually be made up of a few dynamical modes with highly energetic, phase-locked soliton wave packets. In support of this explanation is the fact that the 1st and 2nd horizontal-current EOFs are highly

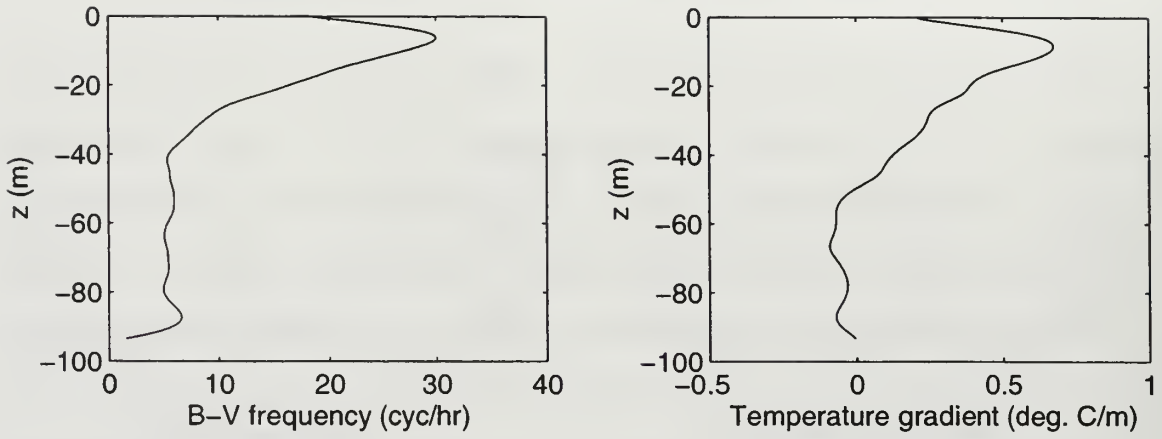


Figure 6. A Brunt-Vaisala frequency profile (left) and a temperature gradient profile (right). Both profiles are derived from a CTD cast taken between the two ADCP sites with some smoothing.

correlated with correlation coefficients larger than 0.7 at both the Shallow and Deep Sites. The empirical decomposition was able to discern these modes in u and v because of the more energetic tidal motions. But the tides, including the internal ones, have little signature in w. It was also found that an almost perfect fit to the EOF for w can be obtained using only the first three dynamical modes, with the first baroclinic mode being the dominant mode in such a fit.

3. Temporal Filtering

The velocity modal-amplitude time-series were then filtered using lowpass, bandpass and highpass Butterworth filters, thereby dissecting the motions into three distinct frequency bands. These three frequency bands are hereafter referred to as:

1. "synoptic," with periods longer than 18 hours,

2. "tidal," with periods between 5 and 18 hours, and

3. "buoyancy," with periods shorter than 5 hours.

The synoptic band should include oscillations directly related to the synoptic weather pattern as well as inertial waves. The tidal band should consist of semi-diurnal tides. The internal waves including the non-linear solitons are expected to reside in the buoyancy band. Figures 7 and 8 show some of the filtered Deep-Site modal horizontal currents in the tidal and buoyancy bands, for two recording periods, JD 208 through JD 212.5 and JD 212.5 through JD 217, respectively. The observed relations between the large-amplitude solitary wave packets, the barotropic and internal tides, and the synoptic atmospheric forcing are to be discussed in the next section.

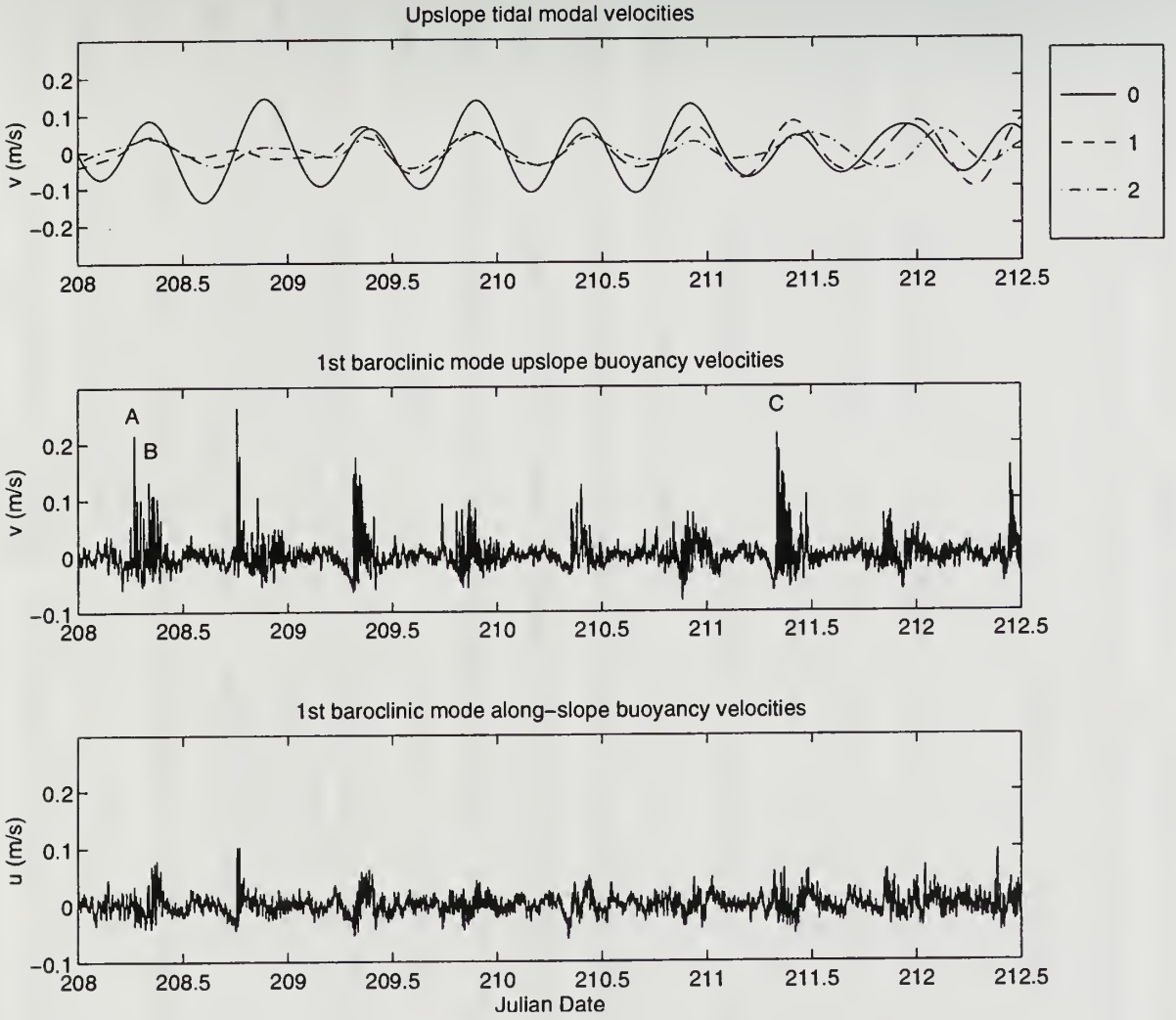


Figure 7. A segment of the observed Deep-Site modal amplitudes between JD 208 and 212.5, showing (top) the upslope tidal currents of the barotropic (solid line) and the 1st (dashed line) and 2nd internal (dot-dashed) modes, (middle) the upslope buoyancy currents of the 1st mode, and (bottom) the along-slope buoyancy currents of the 1st mode, respectively. In the middle panel, three of the soliton packets are labeled as A, B and C.

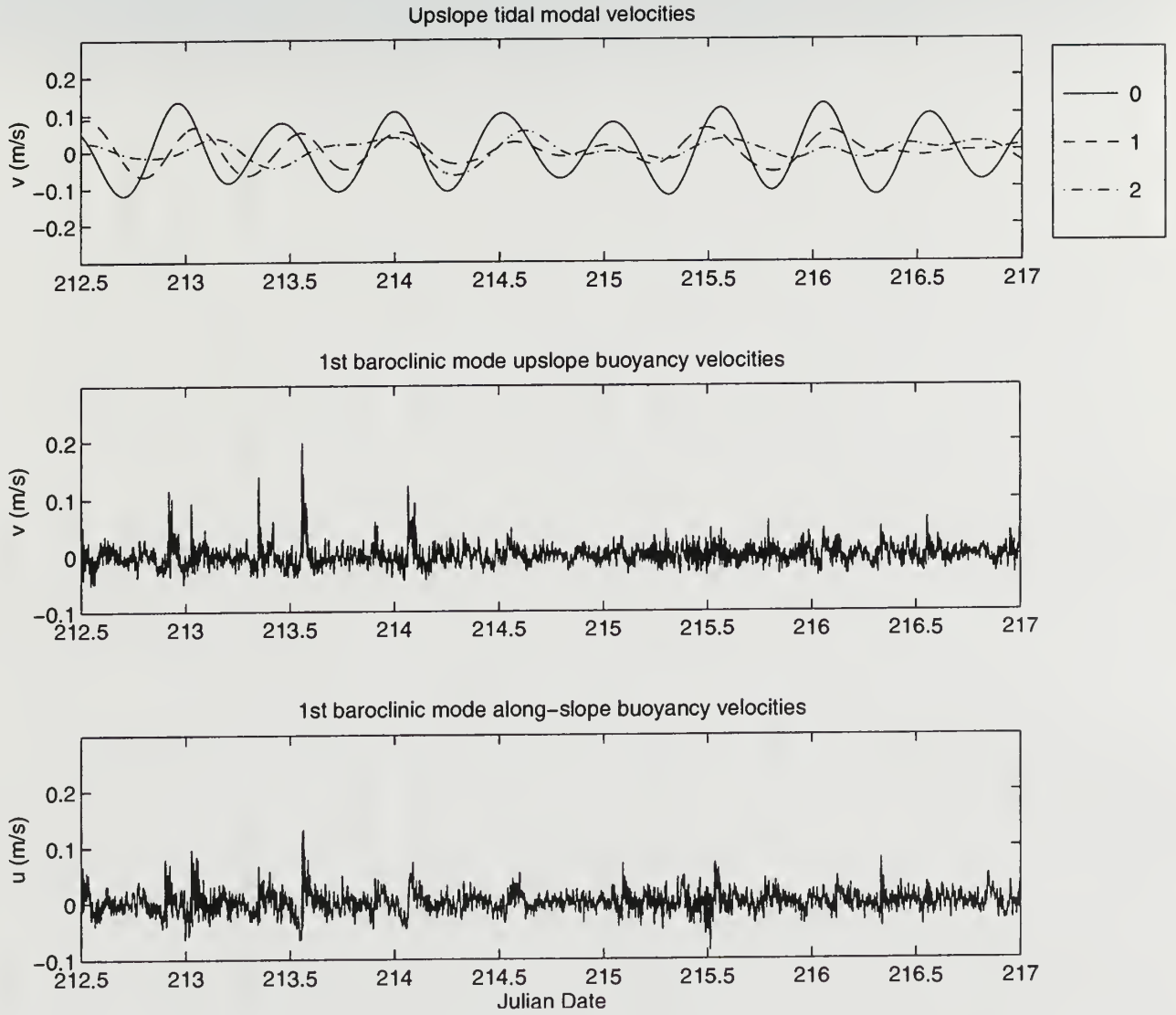


Figure 8. Same as Figure 7, but for the segment between JD 212.5 and 217.

III. ANALYSIS

A. GENERATION

The ADCP data reveal that there were multiple soliton generation sites in the vicinity of the experimental track, as one might surmise after viewing satellite SAR imagery, Figure 4. From the u and v buoyancy-band modal time-series, as displayed in the bottom two panels of Figures 7 and 8, it will be shown that one of the dominant sites of generation was directly off the shelfbreak adjacent to the Deep-Site ADCP. The solitons generated near the Deep-Site ADCP propagated directly upslope (i.e., in the y direction) showing significant signatures in the v component but not in the u component. Examples of these locally generated soliton packets are denoted by "A" and "C" in Figure 7. In the same figure, an example soliton packet that was not generated near the Deep-Site ADCP, but was generated to the southwest of the experimental region, is labeled "B". This "B" packet had a u component of comparable speed to that of the v component. The overall environmental condition was extremely complex, with distantly generated soliton packets also influencing the local condition, either as isolated events or by interfering with the locally generated packets. This complexity is more apparent in the Shallow-Site ADCP data as the distantly generated solitons tended to have larger amplitudes there. Those distantly generated soliton

packets appeared to come primarily from the southwest and the south-southwest. Further analysis in conjunction with the SAR data could help to localize where these distant sites are.

The top panel of Figure 7 depicts a period when the barotropic and internal tides are in-phase in the upslope direction at the Deep-Site, at least until approximately JD 211.5. This was a period when the distantly generated solitons were weak and sometimes absent and the locally generated solitons predominated. These soliton packets rode on the leading edge of the internal tides and coincide with the onset of the barotropic tide. However, as shown in Figures 7 and 8, between JD 211.5 and JD 214.5, the distantly generated solitons appeared more frequently and caused considerable interferences. The distantly generated solitons became difficult to isolate from the locally generated ones. It was also observed that, in this period, the barotropic and internal tides are not exactly in phase. This is probably due to the interferences between the internal tides, upon which the solitons, emanating from the multiple source sites, initially rode.

The generation of solitons in the region of the shelf-break may be explained by different, although not necessarily competing, hypotheses and observations. Apel *et al.* (1995) suggested two possible mechanisms for the generation: coupling of energy between tidal modes and the

release of a standing lee wave off the shelfbreak. In the former generation mechanism, energy from the barotropic tide is scattered into the internal modes within the tidal band at the shelf break as the mode angle of the internal propagation characteristics coincides with the angle of the shelf slope. The internal tides then scatter energy non-linearly into the buoyancy band as they propagate shoreward. For reasons explained below, this is not expected to be the generation mechanism.

The latter mechanism may explain observations of soliton-like internal waves by Loder et al. (1992) and Brickman and Loder (1993) in the region of the Northern Georges Bank shelf break. In this hypothesis, a steady offshore flow, usually provided by the ebbing barotropic tide, is required to establish a spatially oscillating depression (i.e., lee waves) in the pycnocline directly offshore from the shelf break. These depressions are a result of the sudden increase of the relative vorticity caused by the stretching of the water column. The lee wave is eventually released from its phase locked position when the flow reverses. At the onset of the flow reversal, which typically occurs at slack tide, the lee waves, then, travel up the shelf as internal tides coupling energy into the buoyancy band as soliton wave packets. In the absence of Ekman flow, both generation mechanisms would produce common signatures in the ADCP observation, in that soliton packets

would be generated at the onset of the flood cycle of the barotropic tide, and that they would be riding on the leading edge of the internal tides propagating upslope. However, as described below, a synoptic wind event existed during the experiment, allowing us to discard the former hypothesis.

In Figure 9, the upslope component of the synoptic barotropic current is superimposed onto the upslope tidal current. The synoptic current shows that a weather pattern started to move in or develop at approximately JD 214, and is confirmed by wind speed readings provided in Figure 10. This storm event introduced a synoptic shoreward flow which gradually ramped to a peak in excess of 0.3 m/s. This synoptic event suppressed and eventually negated any offshore flow through the end of the ADCP recording. Of note is that during this late period, no solitons were locally generated despite strong tidal flow. The implication is that the generation mechanism is consistent with the lee-wave hypothesis.

B. DYNAMICAL MODAL RELATIONS

Central to the subsequent analyses of the ADCP data on soliton propagation and spectral characteristics is the establishment of the relations between modal displacements and modal horizontal and vertical particle velocities. These important relations, along with some theoretical vertical-structure calculations, are summarized in this

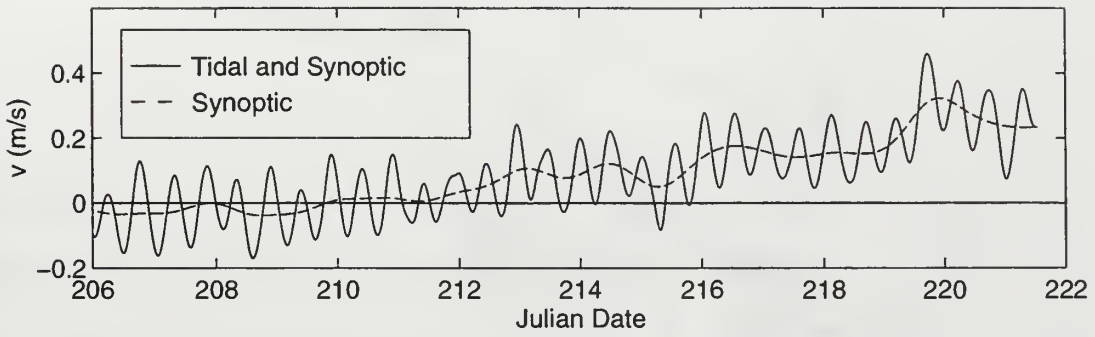


Figure 9. Upslope synoptic currents (dashed line) with tidal currents superimposed (solid line), showing the onset of a synoptic storm event at approximately JD 214 that prevents any offshore flows in the later period. The time-series shown here correspond to the modal amplitudes of the barotropic mode.

section.

The particle velocities (u, v, w) and displacements (η) associated with the ocean variability can be decomposed as linear combinations of vertical modes:

$$(u,v)=\sum_n [u_n(x,y,t),\ v_n(x,y,t)]\ q_n F_n(z) \tag{3a}$$

$$w=\sum_n w_n(x,y,t)\ W_n(z) \tag{3b}$$

$$\eta=\sum_n \eta_n(x,y,t)\ W_n(z) \tag{3c}$$

where F_n and W_n are the vertical modes of horizontal motion and vertical displacement or motion, respectively, q_n arethe normalization constants for F_n, and u_n, v_n, w_n and η_n are the corresponding modal coefficients (i.e., amplitudes) describing the temporal and horizontal structure. For internal disturbances, the vertical-displacement modes W_n

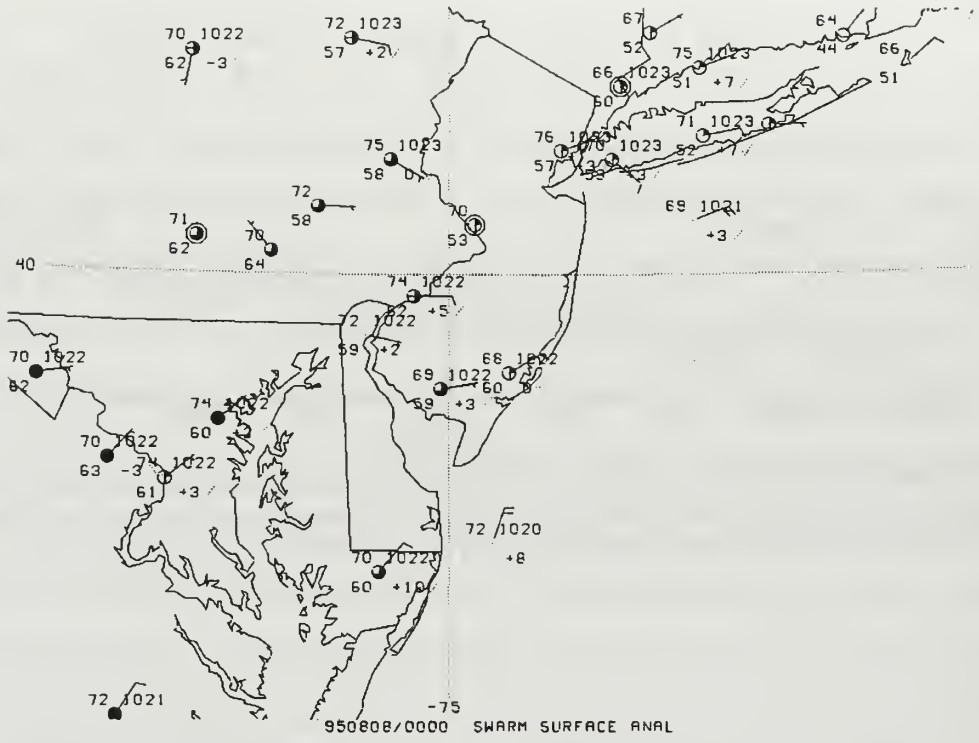


Figure 10. Meteorological data for Julian Date 221 showing wind speeds from land stations and buoys in the vicinity of the experimental site. The buoy reports display winds of 20 knots generally from the NNE and NE.

are governed by the Sturm-Liouville equation:

$$\frac{d^2}{dz^2}W_n + \frac{N^2(z)}{c_n^2}W_n = 0 \tag{4a}$$

subject to the rigid-lid boundary conditions:

$$W_n(0) = W_n(-H) = 0 \tag{4b}$$

where N is the buoyancy frequency, c_n are the eigenvalues which are the modal phase speeds of linear waves in a nonrotating fluid, i.e., for wave frequency much higher than the inertial frequency, and H is the water depth.

The vertical modes of horizontal and vertical motions are related by

$$F_n = \frac{dW_n}{dz} \tag{5}$$

and according to the Sturm-Liouville conditions, they satisfy the following orthogonal conditions:

$$\int_{-H}^{0} N^2 W_n W_m dz = 0; \quad m \neq n \tag{6a}$$

and

$$\int_{-H}^{0} F_n F_m dz = 0; \quad m \neq n \ . \tag{6b}$$

Our choices for normalization are

$$\frac{1}{H}\int_{-H}^{0} W_n^2 dz = 1 \tag{7a}$$

and

$$\frac{1}{H}\int_{-H}^{0} F_n^2 dz = \frac{1}{q_n^2} \ . \tag{7b}$$

With such normalizations, the modal coefficients have the physical meanings of phase-preserved, root depth-averaged square quantities. The 1st and 2nd dynamical baroclinic modes of horizontal current (i.e., F_1 and F_2) and of

vertical displacement or current (i.e., W_1 and W_2) are shown on the top panels of Figure 5. These theoretical vertical structures were calculated based on a buoyancy profile observed by a hydrographic station between the two ADCP sites. This buoyancy profile along with the associated temperature gradient profile are shown in Figure 6. It is seen that the buoyancy frequency ranges from approximately 5 cycles/hr near the bottom to a maximum of 30 cycles/hr in the thermocline with a columnar average of about 10 cycles/hr. It is also seen that the temperature gradient can be as large as 0.7 °C/m at the thermocline, implying that a 10-m internal wave can cause a 7 °C temperature change and a 15-m wave can produce temperature fluctuations as much as 10.5 °C. Such large fluctuations are often seen in the thermistor-chain records during the passage of soliton wavepackets. [Lynch, personal communication]

Using the modal expansion in the fundamental hydrodynamics equations, neglecting rotational effects and energy exchange (i.e., coupling) between modes, and assuming weakly nonlinear, plane progressive waves propagating in a specific direction, Ostroskiy (1978) and Apel *et al.* (1995) have shown that the modal displacements h_n are governed by the KdV equation:

$$\frac{\partial \eta_n}{\partial t} + c_n \frac{\partial \eta_n}{\partial y'} + \alpha_n \eta_n \frac{\partial \eta_n}{\partial y'} + \beta_n \frac{\partial^3 \eta_n}{\partial y'^3} = 0 \qquad (8a)$$

where y' is the direction of propagation of the wavefront, and

$$\alpha_n = \frac{3c_n q_n^2}{2H} \int_{-H}^{0} F_n^3 \, dz \tag{8b}$$

and

$$\beta_n = \frac{c_n q_n^2}{2} \tag{8c}$$

are environmental parameters accounting for the effects of buoyancy, current, current shear and water depth. To 3rd-order, the modal displacements and particle velocities obey the relations (Ostroskiy, 1978):

$$\frac{\partial \eta_n}{\partial t} + q_n \frac{\partial v'_n}{\partial y'} + \frac{s_n}{2} \frac{\partial (\eta_n v'_n)}{\partial y'} = 0 \tag{9a}$$

with

$$s_n = \frac{q_n^3}{H} \int_{-H}^{0} F_n^3 \, dz \tag{9b}$$

where v'_n is the particle velocity parallel to y', and

$$w_n = \frac{\partial \eta_n}{\partial t} + k_n q_n v'_n \frac{\partial \eta_n}{\partial y'} - k_n \eta_n \frac{\partial \eta_n}{\partial t} \tag{10a}$$

with

$$k_n = \frac{\int_{-H}^{0} N^2 W_n^2 F_n \, dz}{\int_{-H}^{0} N^2 W_n^2 \, dz} \quad . \tag{10b}$$

The parameters s_n and k_n express the degree of non-linearity in the relations between η_n and v'_n and η_n and w_n, respectively.

C. SOLITON PROPAGATION

For small amplitude modal displacements, the 3rd and 4th terms of the KdV equation (9) are negligible. In such case, the solution is that of the linear internal waves propagating at phase speeds of c_n. However, for displacements having large enough amplitudes and steepness, the KdV equation admits the well-known soliton solution

$$\eta_n^{(s)} = \eta_{0,n} \, sech^2 \left(\frac{y' - C_n t}{\Delta_n} \right) \tag{11a}$$

where $\eta_{o,n}$ is the peak modal amplitude of the soliton. The superscript (s) is used hereafter to denote modal amplitudes associated with solitons. The soliton has a nonlinear characteristic width:

$$\Delta_n = \sqrt{\frac{12\beta_n}{\alpha_n \eta_{0,n}}} \tag{11b}$$

and propagates with a nonlinear phase speed

$$C_n = c_n + \frac{\alpha_n \eta_{0,n}}{3} \quad . \tag{11c}$$

Both the soliton characteristic width and phase speed depend on the soliton peak displacement. The characteristic width is inversely proportional to the square root of $\eta_{o,n}$ whereas the phase speed is linearly proportional to $\eta_{o,n}$. The implication is that the larger the peak displacement, the faster the soliton propagates and the narrower, or steeper, the soliton is.

Using (9) and (10) and the soliton displacement solution, one can easily obtain the corresponding soliton modal horizontal and vertical velocities. Neglecting 3rd and higher order nonlinear terms, they are:

$$v_n^{(s)} = \frac{C_n}{q_n} \eta_n^{(s)} \left(1 - \frac{s_n}{2q_n} \eta_n^{(s)}\right) \tag{12}$$

and

$$w_n^{(s)} = \frac{\partial \eta_n^{(s)}}{\partial t} \left(1 - 2k_n \eta_n^{(s)}\right) \tag{13}$$

where

$$\frac{\partial \eta_n^{(s)}}{\partial t} = \frac{2C_n}{\Delta_n} \eta_{0,n} \, sech^2\left(\frac{y' - C_n t}{\Delta_n}\right) \tanh\left(\frac{y' - C_n t}{\Delta_n}\right) \quad . \tag{14}$$

Using these soliton modal relations with environmental and

non-linear parameter values calculated based on the observed buoyancy frequency profile, predictions on the evolution of solitons can be attempted. To illustrate the predicted temporal structure of a soliton and the dramatic effect of non-linearity, a soliton solution with a 10-m peak modal displacement along with the corresponding modal horizontal and vertical velocities are displayed in Figure 11. Of particular interest is the dot-dashed curve in the first panel. This curve represents the linearized solution associated with the particle velocities displayed in the lower panels of Figure 11. Clearly, the non-linear advective effect is important as it significantly enhances the displacement. The modal soliton solutions for the first two baroclinic modes are always positive. The positive sign is entirely consistent with the data. In view of the corresponding mode functions shown in Figure 5, the positive sign implies that the solitons in Mode 1 cause only depressions of the isotherms over the entire water column. Whereas for Mode 2, it is a depression below 20 m. Figure 12 shows the predicted dependence between soliton peak modal horizontal current, peak modal vertical current and peak displacement. Again, the predicted relation between the soliton peak horizontal and vertical currents is rather consistent with the data. The observed peaks of the Mode 1 soliton vertical current range from 2 cm/s to 10 cm/s whereas the corresponding horizontal currents have

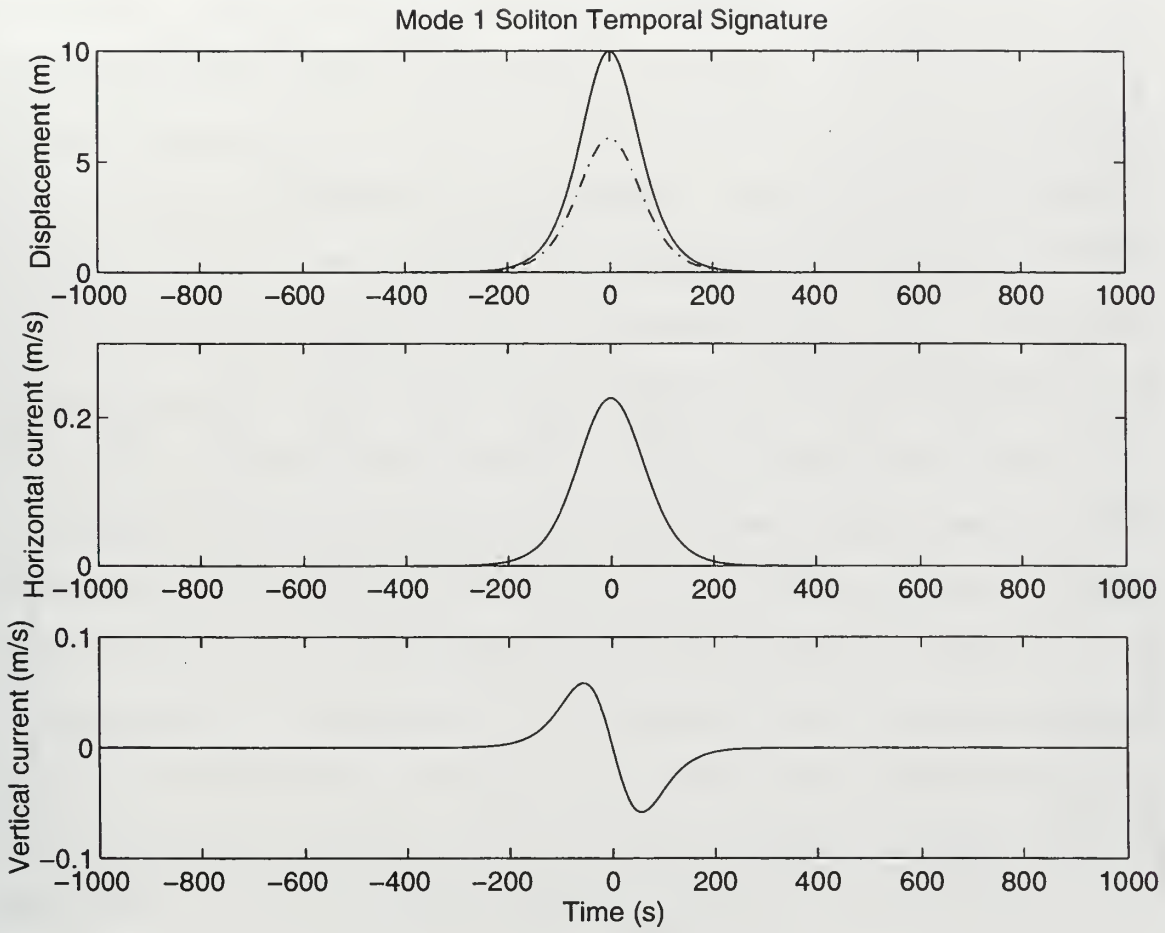


Figure 11. The evolution of modal displacement (top), horizontal current (middle) and vertical current (bottom) associated with a single soliton. The soliton temporal structure (solid lines) was calculated based on weakly non-linear theory. The dot-dashed line in the top panel represents the result of linearization, showing large error.

peaks between 5 cm/s and 30 cm/s. It is interesting to point out that the caps of these observed current peaks coincide roughly to where the predicted curve of peak vertical current versus displacement turns (see bottom panel of Figure 12). This turning of the curve corresponds to where the weakly non-linear soliton theory starts to fail and where the third- and higher order terms become

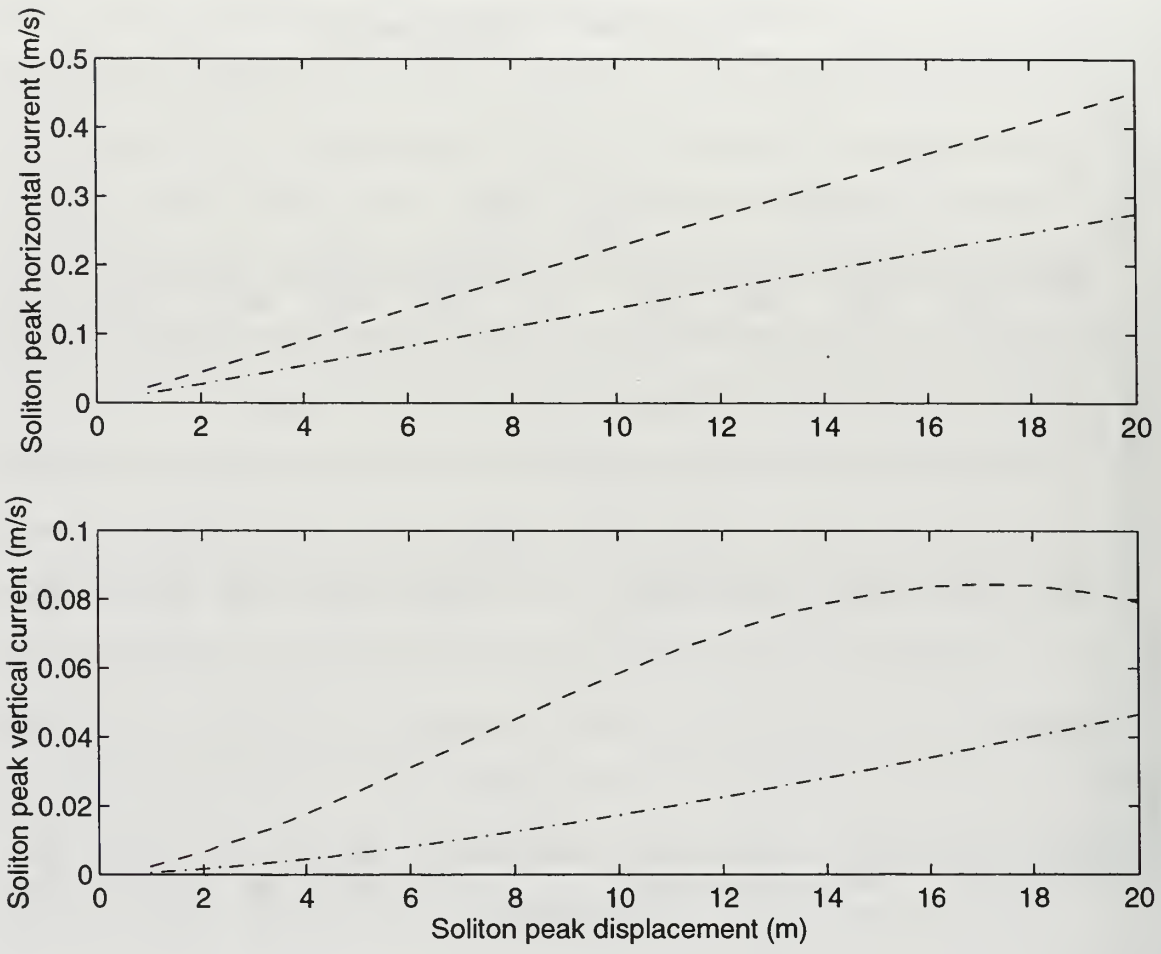


Figure 12. Theoretical relations between soliton peak displacement and (top) peak horizontal current, and (bottom) peak vertical current for the first (dashed lines) and second (dot-dashed) baroclinic modes.

important. Near this cap, the solitons are extremely steep (i.e., narrow) with displacements exceeding 15 m. It is not unlikely that they would break and contribute significantly to vertical mixing.

The alignment of the two ADCPs with the adjacent soliton generation site has allowed for a verification of the theoretical soliton phase speed as passage times at two ADCPs which were separated by a known distance could be

observed. Before the onset of the synoptic storm event which mitigated the production of solitons, there was a common time period, JD 209.5 through JD 216.5, in which both ADCPs were recording simultaneously. Using this five-day segment of the time-series, it was possible to track a total of eight non-interfered soliton wavepackets in the first EOF that were generated off the immediate shelfbreak (i.e., with relatively small u velocities). While the travel time from the Deep Site to the Shallow Site of the leading soliton in each packet provided an estimate of its phase speed, its peak vertical velocity provided estimate of its peak displacement. The results are marked by circles on the top panel of Figure 13, in which the theoretical phase-speed curves for the 1st and 2nd dynamical modes are also displayed. Qualitative agreement is noted between the observed phase speeds and the predicted phase speeds of the 1st baroclinic mode. This is not surprising because the EOF for displacement (w) is mostly matched by the 1st dynamical mode. A real surprise, however, is the high correlation (above 0.7) between the modal amplitudes of the 1st and 2nd EOFs of the buoyancy-band upslope horizontal current (v), at both the Deep and Shallow Sites. High correlation was only anticipated at the Deep Site but not the Shallow Site, which was more than 16 km away from where the soliton packets were generated. The implication is that Mode 2 did not propagate with the much smaller phase speed in accord with the weakly

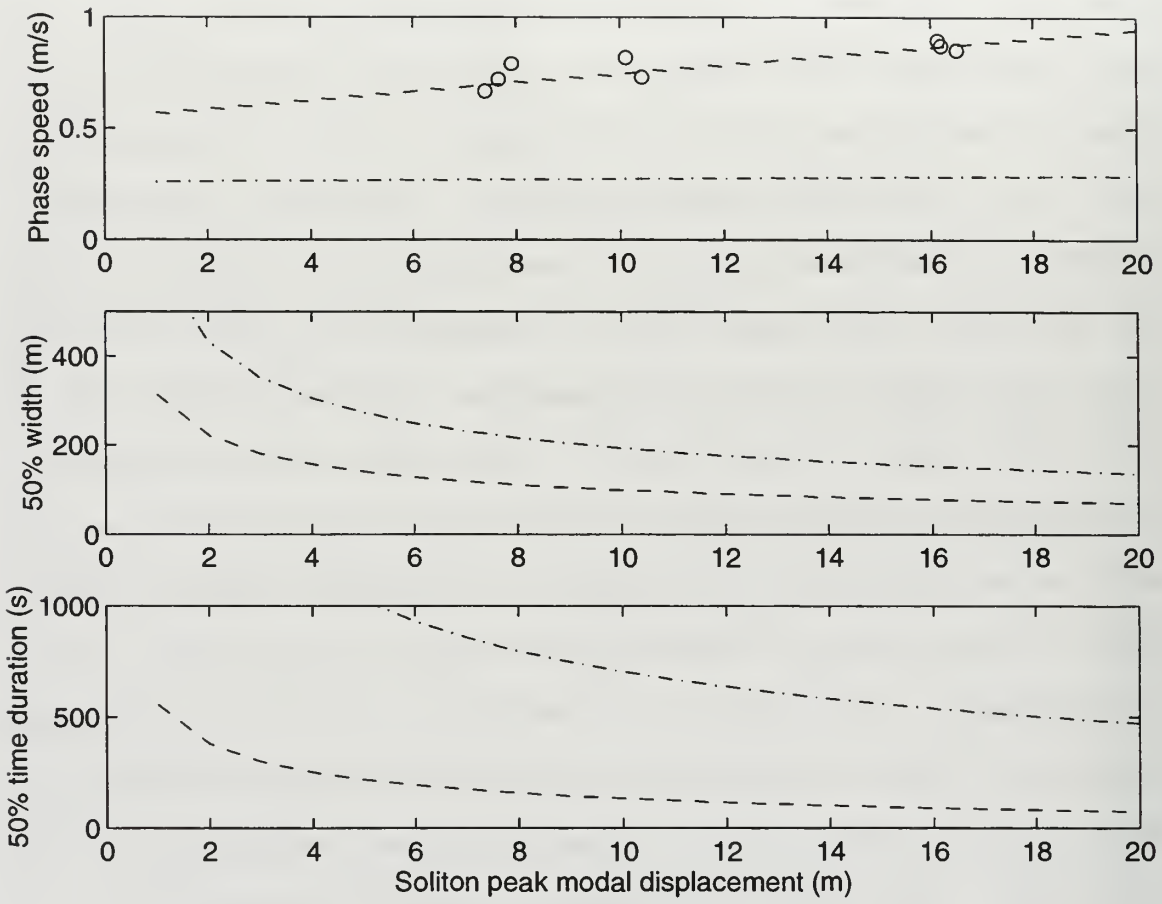


Figure 13. Theoretical relations between soliton phase speed (top), 50% width (middle) and 50% time duration (bottom) and peak modal displacement for the first (dashed lines) and second (dot-dashed lines) baroclinic modes. Observed soliton phase speeds are indicated by circles showing agreement with the predicted first-mode phase speed.

nonlinear, de-coupled soliton theory. Instead, it propagated together with Mode 1. A phase-locked mechanism apparently existed. Therefore, an outstanding question is what causes this phase-locked behavior. Could it be due to mode coupling such that Mode 1 replenished the Mode 2 energy along the way? Could it, instead, be due to higher-order non-linearity, since the phase speeds and particle speeds of Mode 2 have the same magnitude? Or, lastly, might it be due

to tidal shear which may have strongly modified the tidal band vertical mode structure? These questions remain open for future investigations.

In the bottom two panels of Figure 13, the predicted 50% width and time duration, for both Modes 1 and 2, as a function of the soliton peak modal displacement are plotted. We use "50%" to denote where, or when, the displacement drops to 50% of its peak value. The theoretical curves for Mode 1 suggested that the observed solitons should have 50% widths of about 100 to 200 m and 50% time durations of about 100 to 300 s. These width and duration estimates are consistent with observations.

D. DISPLACEMENT POWER SPECTRAL DENSITY

The displacements of isotherms are directly related to sound-speed perturbations. Therefore, for underwater acousticians, the power spectral density of displacements is a more preferable characterization of the acoustic random medium than those of the particle velocities. In this spirit, an attempt to provide some estimates and discussion of the displacement power spectral density will be presented next.

Displacement time-series can be derived from the vertical-current time-series. The relation between modal vertical velocity and modal displacement as stated in (13) can be integrated to give

$$\eta_n - k_n \eta_n^2 = \int w_n \, dt \quad . \tag{15}$$

It is noted that this integral relation for solitons is also valid for linear internal waves residing in the energy-containing frequency band of the soliton packets. For these linear waves, the nonlinear $k_n\eta_n^2$ term is much smaller than η_n and hence contributes little in the overall equation. The soliton energy-containing band can be easily estimated by performing a Fast Fourier Transform (FFT) on just a few individual soliton packets. Such a band is 40 cycles/day and above. Therefore, if it is assumed that the greater-than-40-cycles/day ocean variability consists of linear internal waves and solitons only, (15) can be used to convert the observed vertical currents into displacements in this band.

Thus, the procedure in obtaining the modal displacement time-series involved, as a first step, filtering the observed modal vertical velocity into a lowpass time-series and a highpass time-series, both with a cutoff at 40 cycles/day. After integrating both series in time, the highpass one was then corrected, based on (15) through polynomial root finding. Finally, the lowpass and corrected highpass displacement series were added to give the overall displacement time-series. Partial segments of the corrected, highpass modal displacements at both the Shallow and Deep Sites are shown in Figure 14. Having a common time

window, the two segments show the evolution of four soliton packets over two tidal cycles. Although it may be difficult to see without the aid of the horizontal currents, there were actually two packets per cycle with the locally generated packet leading.

With the expectation that the spectral characteristics would be dissimilar between time periods with little soliton activities and those with heavy activities, it is only logical to treat the active and inactive periods separately in the spectral estimate. The displacement time series were carefully cut into many non-overlapping sections, each six hours long. The six-hour window was chosen because each soliton packet was typically four to six hours long. For each ADCP, the six-hour sections were then assembled into two groups, one with soliton packets and the other without soliton packets. The spectral density of each group was then estimated through ensemble averaging of the magnitude squared sectional FFTs.

Figure 15 shows the resultant power spectral density estimates of the modal displacements, at the Shallow and Deep Sites, for periods with and without soliton activities. For the solitonless periods, both the Shallow and Deep-Site spectra exhibit a frequency dependence of approximately $f^{-3/2}$ over the band from 10 to 150 cycles/day. But beyond 150 cycles/day (i.e., the buoyancy frequency), the solitonless spectrum falls off much more gradually in the Shallow Site

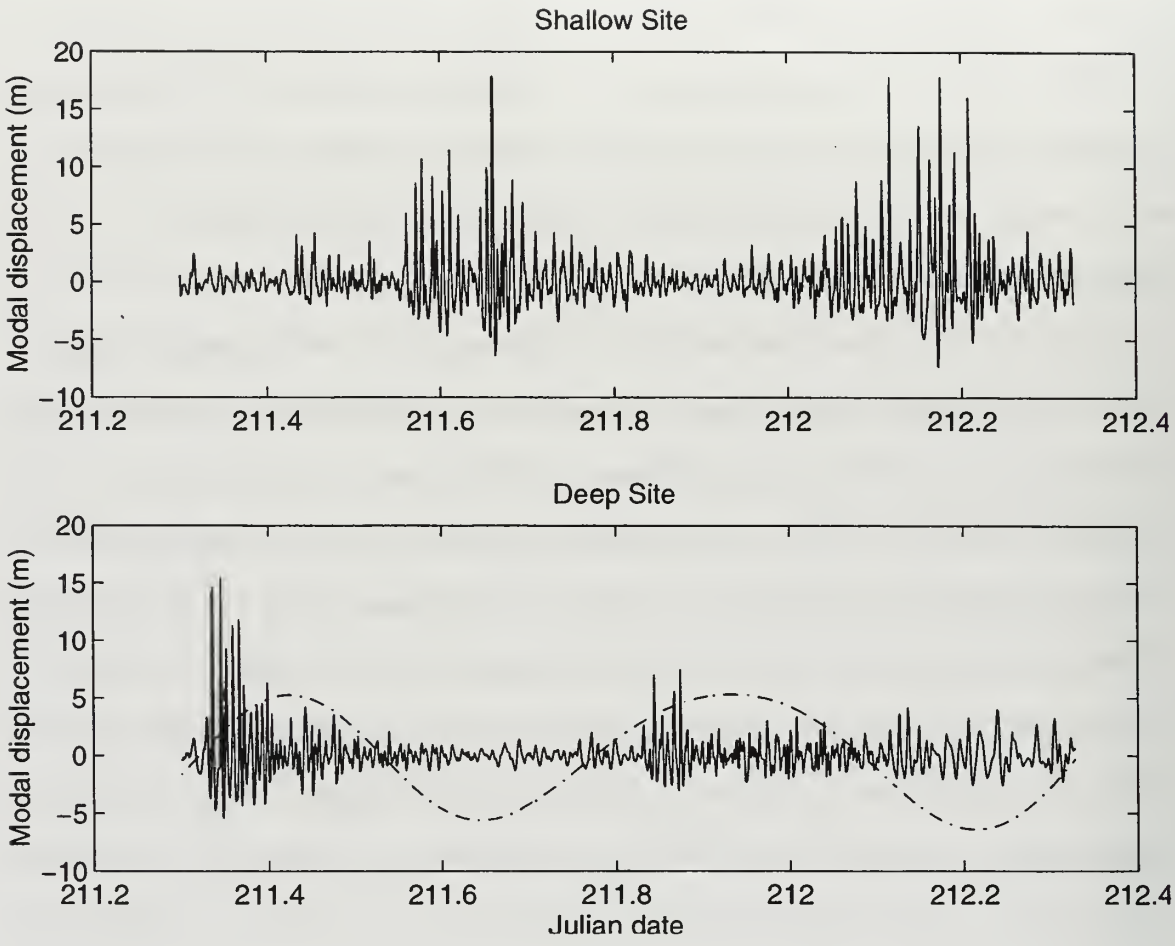


Figure 14. A segment of highpass time-series of modal displacements, at the Shallow (top) and Deep (bottom) Sites. The upslope barotropic tidal current (dot-dashed line in units of cm/s) is superimposed to show that this segment encompasses two tidal cycles with strong soliton packets generated near the Deep Site during the tidal flood.

than in the Deep Site. The $f^{-3/2}$ dependence below 150 cycles/day is rather remarkable in that the same dependence was observed by Lynch *et al.* (1996) in the Barents Sea. Since the Barents Sea is also on a large shelf, but at much higher latitude, the commonality of this $f^{-3/2}$ dependence for shelf regions is an interesting question to ask.

It is apparent from Figure 15 that the spectral effects

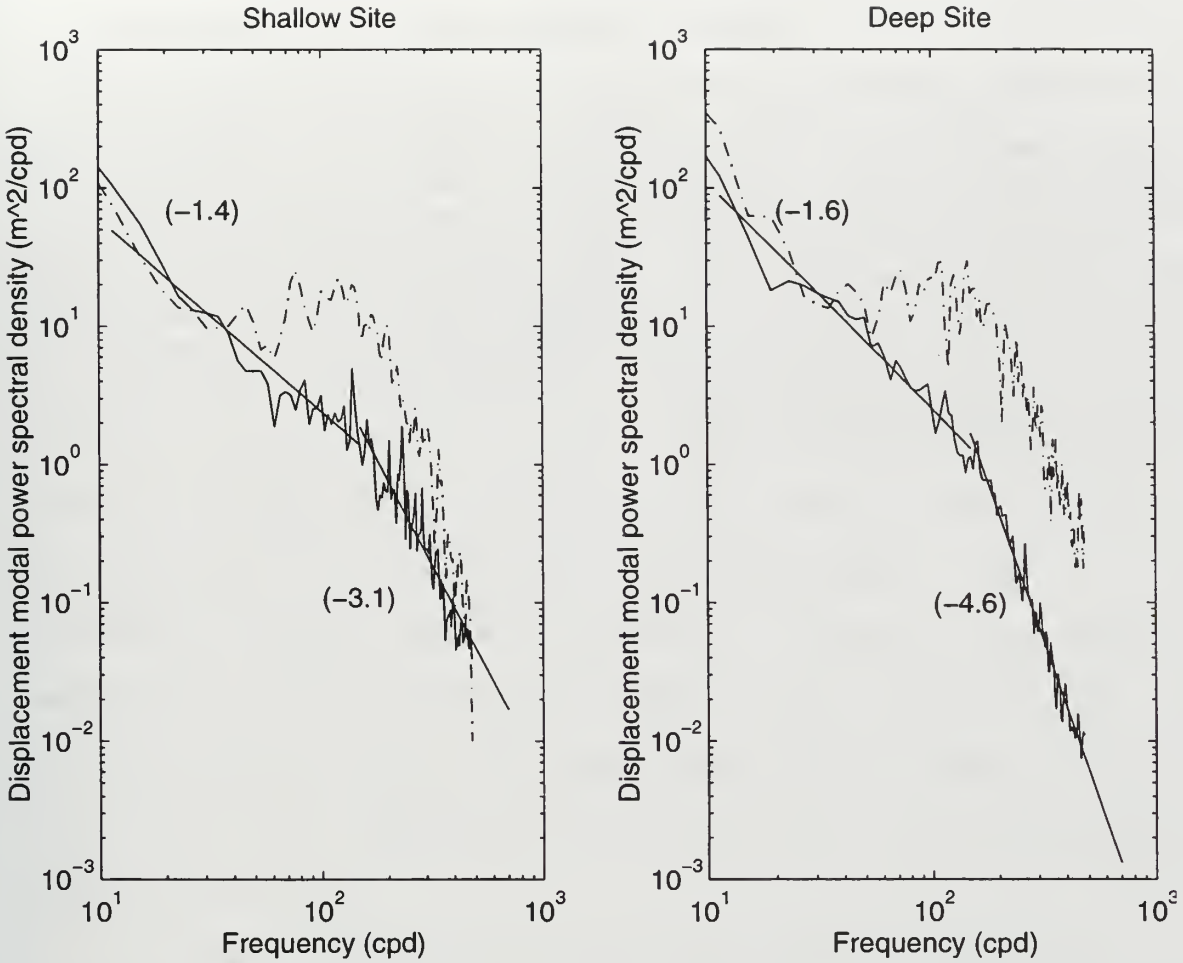


Figure 15. Power spectral density estimates for periods with no soliton activities (solid curves) and periods of strong soliton activities (dot-dashed curves) for both the Shallow (left panel) and the Deep (right panel) Sites. The solid straight lines represent linear least-squares fit to the solitonless logarithmic spectra in two different frequency bands. The slopes of these fits are shown in parentheses.

of the soliton packets include the elevation and whitening of the band from 40 to 200 cycles/day with slight resonance toward the higher end of this band. This slight resonance is associated with the full durations of the individual solitons. For peak modal displacements of 8 to 10 m, the soliton full durations are predicted by theory to be approximately between 600 and 500 s. The reciprocals of these durations give 140 to 170 cycles/day. The spectral

elevation is significant, revealing an order-of-magnitude increase of potential energy in this elevated band. It was also observed that the soliton-active spectral density falls off much more rapidly beyond 200 cycles/day at the Shallow Site than at the Deep Site. This difference might very well be due to the breaking of the high-amplitude solitons as they propagated shoreward.

IV. CONCLUSIONS

Analysis of the nearly 3 week-long ADCP records obtained during the summer near the shelf break in the Mid-Atlantic Bight reveals that non-linear internal waves are evident and appear to be generated at multiple source sites in the vicinity of the SWARM '95 experimental site. It was observed that generation of non-linear internal waves ceased when the off-shelf tidal flow was countered by atmospheric forcing during the later part of the experiment. The atmospheric forcing induced a synoptic shoreward flow which negated any offshore flow coincident with a cessation of soliton generation near the experimental site. These observations are consistent with the lee-wave hypothesis for soliton generation.

A further finding from the time-series was that the observed phase speed of the solitons was in good agreement with predicted phase speeds of the first baroclinic mode. This was not surprising as the EOF for displacement is mostly matched by the first dynamical mode. What was surprising was the strong correlation between the modal amplitudes of the 1st and 2nd EOFs of the buoyancy band upslope horizontal current (v) at both the Deep and Shallow Sites. This implied that the 2nd EOF propagated phase-locked with the 1st EOF.

Lastly, the displacement power spectral density

estimates of the soliton-active periods and the solitonless periods provided a look at the potential energy associated with solitons. First, an increase of potential energy in the soliton-active spectrum is apparent when compared with the solitonless spectrum. Another point is that the soliton-active spectral density falls off much more rapidly beyond 200 cycles/day at the Shallow-Site than at the Deep-Site. This difference may be caused by breaking of the high amplitude solitons as they propagate upslope.

In order to further the understanding and characterization of solitons in SWARM '95, it will be necessary to include the other, complementary, data sets in future analyses. Hydrodynamic models of the wave packets may serve as a framework for a joint analysis of the different observations. The study of the impact of solitons on acoustic signals may then be enhanced. A further goal will be to, eventually, predict soliton generation, propagation and dissipation. Hopefully, this will lead to predicting the impact of solitons on naval operations.

REFERENCES

Apel, J.R., H.M. Byrne, J.R. Proni, and R.L. Charnell, "Observations of Oceanic Internal and Surface Waves From the Earth Resources Technology Satellite," *J. Geophys. Res.*, Vol. 80, No. 6, 865-881, February 20, 1975.

Apel, J.R., L.A. Ostrovskiy, and Y.A. Stepanyants, "Internal Solitons in the Ocean," Applied Physics Laboratory, Johns Hopkins University, Technical Report MERCJRA0695, 65 pages, July 1995.

Brickman, D. and J.W. Loder, "Energetics of the Internal tide on the Northern Georges Bank," *J. Phys. Oceanogr.*, Vol. 23, 409-424, 1993.

Chereskin, T.K., "Generation of internal waves in Massachusetts Bay," *J. Geophys. Res.*, Vol. 88, No. C4, 2649-2661, March 20, 1983.

Davis, R.E. and Acrivos, A., "Solitary internal waves in deep water," *J. Fluid Mech*, Vol. 29, No. 3, 593-607, 1967.

Farmer, D.A., and J.D. Smith, "Tidal interactions of stratified flow with a sill in Knight Inlet," Deep Sea Res., Vol. 27A, 239-254, 1980.

Holloway, P.E., "Internal hydraulic jumps and solitons at a shelf break region in the Australian North West Shelf," *J. Geophys. Res.*, Vol. 92, No. C5, 5405-5416, May 15, 1987.

Lee, C.-Y., and R.C. Beardsley, "The Generation of Long Nonlinear Internal Waves in a Weakly Stratified Shear Flow," *J. Geophys. Res.*, Vol. 79, No. 3, 453-462, January 20, 1974.

Loder, J.W., D. Brickman and E.P.W. Horne, "Detailed Structure of Currents and Hydrography on the Norther Side of the Georges Bank," *J. Geophys. Res.*, Vol. 97, No. C9, 14,331-14,351, September 15, 1992.

Long, R.R, "Some aspects of the flow of stratified fluids. I. A theoretical investigation," *Tellus*, Vol. 5, No. 1, 42-57, 1953.

Long, R.R, "Solitary waves in one- and two-fluid systems," *Tellus*, Vol. 8, No. 4, 460-471, 1956.

Lynch, J.F., Woods Hole Oceanographic Institution, personal communication, 1996.

Lynch, J.F., J. Guoliang, R. Pawlowicz, D. Ray and A.J. Plueddemann, "Acoustic travel-time perturbations die to shallow-water internal wave and internal tides in the Barents Sea Polar Front: Theory and experiment," *J. Acoust. Soc. Am.*, Vol. 99, No.2, 803-821, February 1996.

Munro, R.G., "First Davis Strait discovery overcomes offshore hazards," *World Oil*, Vol. 194, No. 5, 85-91, April, 1982.

Osborne, A.R., T.L. Burch, and R.I. Scarlet, :The Influence of Internal Waves on Deep-Water Drilling." *J. of Petroleum Tech.*, Vol. 30, 1497-1504, October 1978.

Osborne, A.R., and T.L. Burch, "Internal Solitons in the Andaman Sea," *Science*, Vol. 208, Number 4443, 451-460, May, 2, 1980.

Ostrovskiy, L.A., "Nonlinear internal waves in rotating fluid," Oceanology, Academy of Sciences of the uSSR, Vol. 18, No. 2, 119-125, 1978.

RD Instruments, *Self-Contained Acoustic Doppler Current Profiler (SC-ADCP) Technical Manual, Incorporates Change 2*, September 1992.

Sandstrom, H., and J.A. Elliot, "Internal tide and solitons on the Scotian Shelf: A nutrient pump at work," *J. Geophys. Res.*, Vol 89, No. C4, 6416-6426, July 20, 1984.

Zhou J.-X., X.-Z. Zhang, and P.H. Rogers, "Resonant interaction of sound wave with internal solitons in the costal zone," *J. Acoust. Soc. Am.*, vol. 90, No. 4, Pt 1, October 1991.

INITAL DISTRIBUTION LIST

		No.Copies
1.	Defense Technical Information Center 8725 John J. Kingman Rd., STE 0944 Ft. Belvoir, VA 22060-6218	2
2.	Dudley Knox Library Naval Postgraduate School 411 Dyer Rd. Monterey CA 93943-5101	2
3.	Professor Robert H. Bourke (Code OC/Bf) Oceanography Department Naval Postgraduate School 833 Dyer Rd., RM 324 Monterey CA 93943-5122	1
4.	Professor Robert L. Haney (Code OC/HY) Meteorology Department Naval Postgraduate School 589 Dyer Rd., RM 252 Monterey CA 93943-5114	1
5.	Dr. Ching-Sang Chiu (Code OC/Ci) Oceanography Depaartment Naval Postgraduate School 833 Dyer Rd., RM 318 Monterey CA 93943-5122	4
6.	Dr. Thomas H.C. Herbers (Code OC/He) Naval Postgraduate School 833 Dyer Rd., RM 331B Monterey CA 93943-5122	1
7.	Commanding Officer Naval Ice Center FOB#4, Room 2301 Suitland, MD 20395 Attn: LCDR Donald W. Taube	3
8.	Dr. James F. Lynch Department of Applied Physics and Ocean Engineering Mail Stop #21 Woods Hole Oceanographic Institution Woods Hole, MA 02543-1047	1

9. Dr. Marshall M. Orr 1
Code 7120
Naval Reseach Laboratory
Building 1, Room 400a
4555 Overlook Ave., S.W.
Washington DC, 20375

10. Mr. Todd Anderson 1
Monterey Bay Aquarium Research Institute
Room, A264
P.O. Box 628
Moss Landing, CA 95039-0628

11. Ms. Marla Stone (Code OC/So) 1
Naval Postgraduate School
833 Dyer Rd., RM 331B
Monterey CA 93943-5122

12. Dr. Lou Goodman (Code 322PO) 1
Office of Naval Research
800 North Quincy Street
Arlington, VA 22217

13. Dr. Steve Ramp (Code 322PO) 1
Office of Naval Research
800 North Quincy Street
Arlington, VA 22217

14. Dr. Jeff Simmen (Code 321OA) 1
Office of Naval Research
800 North Quincy Street
Arlington, VA 22217

15. Dr. Ellen Livingston (Code 321OA) 1
Office of Naval Research
800 North Quincy Street
Arlington, VA 22217

DUDLEY KNOX LIBRARY
NAVAL POSTGRADUATE SCHOOL
MONTEREY CA 93943-5101

DUDLEY KNOX LIBRARY
3 2768 00323864 3